IEEE Photonics Journal
An IEEE Photonics Society Publication

Direct Side Pumping of Double-Clad Fiber Laser by Laser Diode Array Through the Use of Subwavelength Grating Coupler

Volume 4, Number 2, April 2012

C. W. Huang
C. L. Chang
D. Y. Jheng
K. Y. Hsu
S. L. Huang, Senior Member, IEEE
D. W. Huang, Member, IEEE

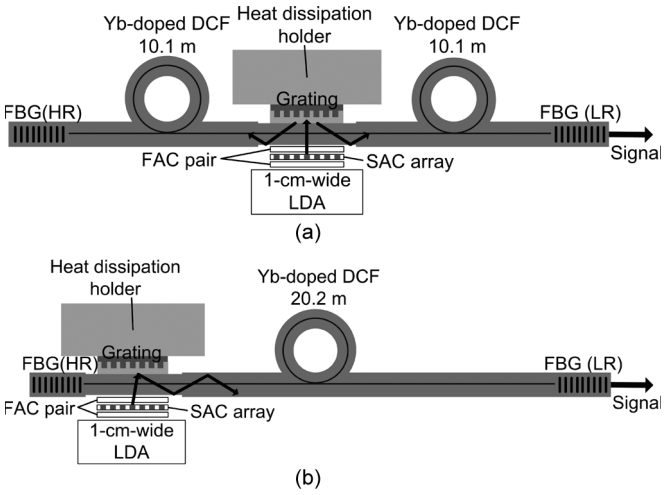

DOI: 10.1109/JPHOT.2012.2186561
1943-0655/$31.00 ©2012 IEEE

Direct Side Pumping of Double-Clad Fiber Laser by Laser Diode Array Through the Use of Subwavelength Grating Coupler

C. W. Huang, C. L. Chang, D. Y. Jheng, K. Y. Hsu, S. L. Huang, *Senior Member, IEEE*, and D. W. Huang, *Member, IEEE*

Graduate Institute of Photonics and Optoelectronics, National Taiwan University, Taipei 10617, Taiwan

DOI: 10.1109/JPHOT.2012.2186561

Manuscript received November 10, 2011; revised January 20, 2012; accepted January 25, 2012. Date of publication February 3, 2012; date of current version March 15, 2012. This work was supported by the Aim for Top University Project from the Ministry of Education, Taiwan, the National Taiwan University Excellent Research Project (10R80908), and the National Science Council (NSC), Taiwan, under the Grants NSC 99-2120-M-002-014, NSC 100-2120-M-002-010, and NSC 100-2221-E-002-134. Corresponding author: D. W. Huang (e-mail: dwhuang@cc.ee.ntu.edu.tw).

Abstract: An electron-beam-fabricated subwavelength grating coupler for direct side coupling of light emission from a high-power laser diode array (LDA) was studied theoretically and implemented experimentally. A gold-embedded silica-based design for grating coupler was employed to minimize the thermal expansion caused by the accumulated heat from light absorption by metal part of the grating coupler. In addition, with the consideration of the backward diffraction loss and the groove wall nonverticality caused by fabrication distortion, the grating pitch and groove width were optimized for the highest coupling efficiency. According to the experimental results, the grating coupler is capable of coupling light power up to 21 W from a 976-nm continuous-wave-operated LDA into the inner clad of a 400-μm-diameter double-clad fiber with an overall coupling efficiency of 50%. Furthermore, an LDA side-pumped ytterbium-doped DCF laser by using the grating coupler was demonstrated. By fine tuning the slow-axis collimation lens array, the laser-pumping scheme can easily be switched between bidirectional pumping and unidirectional pumping. Compared with the unidirectionally pumped fiber laser of the same gain fiber length, the laser slope efficiency of the bidirectionally pumped fiber laser was increased by 18% because of a better gain distribution over the fiber length. Finally, the signal output power of 10 W with a slope efficiency of 61% was achieved for the bidirectional side-pumped fiber laser.

Index Terms: Diode-pumped lasers, gratings, diffractive optics.

1. Introduction

High-power diode-pumped fiber lasers have been advancing rapidly in recent years [1]. It is worthy of noting that the dramatic success in high-power fiber laser technology began from invention of the double-clad fiber (DCF) [2]. The inner cladding supports high capability of pump wave and the doped single mode core induced signal can be diffraction-limited; therefore, the fiber lasers can produce high brightness output using broad area laser diodes (LDs) or laser diode arrays (LDAs) of even higher power [3]–[7]. Among the clad-pumping techniques by LDAs, two basic arrangements have been successfully developed. The first one elaborates on the use of mode-shaping optics to transform the line-shaped LDA optical beams into square or circular shaped modes for launching the light into DCF clad and has become the mainstream technology, such as the beam twister coupler [8], microstep mirror [9], M-block [10], and T-bar [11] methods. The second one utilizes butt-coupling of the individual LDA emitting element to fiber array, followed by a tapered fiber bundle

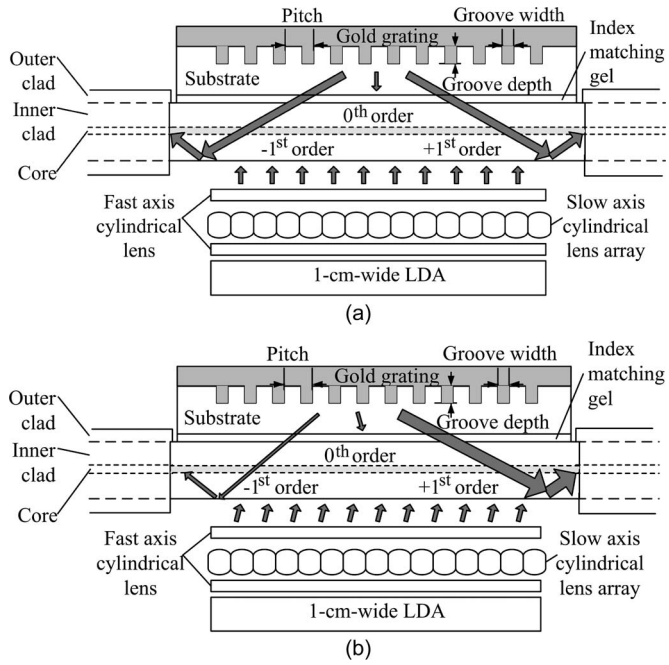

Fig. 1. Schematic diagrams of the gold-embedded silica grating coupler with (a) normal incident pump light, and (b) an angle of incident pump light.

coupler to side launch the optical power into the DCF. Based on such an arrangement, two types of tapered fiber bundle couplers, the nonfused angle-polished fiber coupler [12], [13] and the fused angle-polished fiber coupler [14], [15] have been proposed. In this paper, a more compact and highly efficient clad-pump configuration is implemented. Through a grating coupler, the emission form LDA was directly side launching to DCF clad through a set of brightness preserved focusing/collimating optics. The advantage is that the line-shaped LDA mode is maintained all the way into the DCF clad without reshaping it. In terms of the grating coupling technique for direct coupling of the light from a high-power LDA into a DCF, the difficulties are in the grating fabrication, the physical dimension of the LDA, and the light absorption of the grating coupler; these issues may cause additional problems and need to be considered. It is found that there are two crucial factors to achieve high coupling efficiency for a commercial 1-cm-wide LDA: 1) the thermal expansion caused by the accumulated heat from the light absorption by the metal part of the grating coupler and 2) the backward diffraction of the light which is internally reflected at the fiber boundary. Therefore, a structure of gold-embedded silica was suggested to overcome the thermal problem. Besides, the optimization of grating design parameters is performed to compensate the effect of the lithographic errors, such as the nonverticality of the sidewalls of the grating grooves, results in a coupling efficiency of 50% for high-power operation. Additionally, a side-pumped ytterbium (Yb)-doped DCF laser was also implemented by using the grating coupler. Without using any wavelength-division multiplexing (WDM) couplers, the grating coupler can work as a bidirectional pumping or a unidirectional pumping mechanism by slightly shifting the collimation lens array. Finally, a better laser performance of the symmetrically bidirectional pumping scheme was also observed and compared with the unidirectional pumping scheme.

2. Design of Grating Coupler

Because of the consideration of the thermal expansion of the metal grating, a structure was suggested, which the gold film is embedded in the etched grooves on a silica substrate. The schematic diagram of the gold-embedded silica grating coupler was shown in Fig. 1(a). The fiber used in our experiment is a round shape fiber, and therefore, its cylindrical lens effect was considered in the

TABLE 1
Optimized results of different metal grating at pitch of 680 nm

Material	Optimized diffraction efficiency for the sum of ±1st orders	Optimized groove depth (nm)	Optimized groove width (nm)
Au (Gold)	0.94	130	170
Ag	0.92	125	170
Cu	0.82	125	180
Al	0.80	110	190
Ti	0.26	150	225
Ni	0.37	140	210
Cr	0.23	150	225

design of optical path. The presence of the fiber itself gives us an additional freedom to shape the laser beam that is illuminated on the grating. By tuning the gap between the fiber and the second fast-axis cylindrical lens as shown in Fig. 1, the emission form the LDA can be focused down to a 1-cm-wide and 200-μm-high line-shape beam to be illuminated on the grating in the experiment. The grating structure was assumed to have vertical groove walls. For normal incidence, the pump light will be diffracted into $\pm$1st orders, and the power will be symmetrically distributed for each order. When the cylindrical lens array is slightly shifted, the incident light will become slightly deviated from normal incidence by an angle, and the power distribution of the diffracted $\pm$1st orders will be asymmetrical, as shown in Fig. 1(b). Therefore, most of the coupled light will propagate toward only one direction. For the grating design, it is needed to consider the LDA wavelength and the related grating diffraction angle first, and hence the grating pitch is determined. After the beam size is determined, then the grating diffraction efficiency under a fixed grating pitch can be optimized. The designed diffraction angle for the $\pm$1st orders must be larger than the critical angles both at the fiber's inner clad-air interface and the inner clad-outer clad interface, in order to satisfy the condition for total internal reflection (TIR), so that the laser emission light could be coupled into the inner cladding of the DCF and then guided along the fiber. Since the numerical aperture of the DCF is 0.46 for the cladding modes, a relatively large diffraction angle is required. Although no simple and straightforward design rule has been developed so far, the maximum diffraction efficiency of the grating can be determined by numerical simulation, using the Rigorous Coupled-Wave Analysis (RCWA) technique [16]. Various metals, such as Au, Ag, Cu, Al, Ti, Ni, and Cr, were studied for their suitability as grating materials shown in Table 1.

The simulation results show that, a metal with a complex refractive index with a lower real part and a higher imaginary part results in more efficient diffraction of the $\pm$1st orders. Therefore, gold (Au) was chosen as the material for the grating coupler, because it exhibited the highest efficiency at large diffraction angles. Fig. 2(a) shows the diffraction efficiency for the gold-embedded silica grating coupler as a function of the groove depth and groove width at a grating pitch of 680 nm. The optimized overall diffraction efficiency (the sum of both $\pm$1st orders) is higher than 90% for the TM-polarized incident light. However, the simulation results indicate that 7% of the incident light is absorbed by the gold film and generates heat. The consequent thermal expansion of the grating structure becomes significant as the power of the incident light becomes greater. For this reason, a proper heat dissipation mechanism is essential for the grating coupler to achieve a high coupling efficiency in high-power applications.

The 3-D visualization of the diffraction efficiency for the sum of $\pm$1st orders as a function of the launch angles ϕ (to the plane normal to the direction of the grating grooves) and θ (to the plane normal to the direction of the grating vector) is shown in Fig. 2(b). From the figure, it can be seen that the overall grating diffraction efficiency varies slowly and smoothly as the incident angles of ϕ and θ are smaller than $\pm 1^\circ$ and $\pm 7^\circ$, respectively. When one looks at the diffraction efficiency of $+$1st and $-$1st order individually when the incident angle θ is fixed at 0° and the angle ϕ is varies from 0° to $+1^\circ$, it can be seen that the efficiency of $+$1st order increases to nearly 90%, while that of

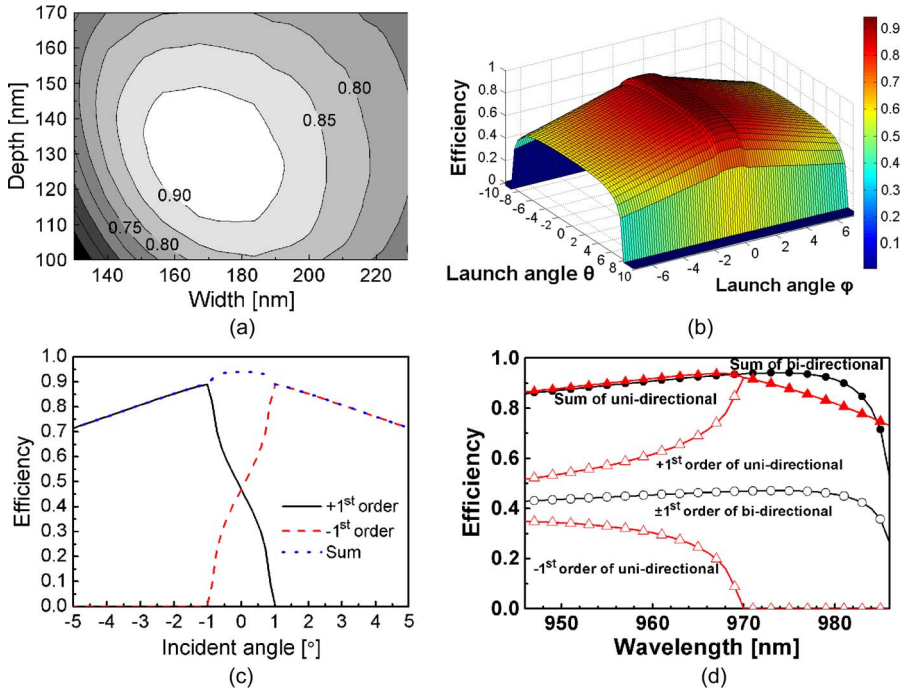

Fig. 2. (a) The sum of both $\pm$1st orders diffraction efficiency of the perfectly vertical walls grating as a function of the groove depth and groove width. (b) The 3-D grating diffraction efficiency with launched angle ϕ and θ. (c) The grating diffraction efficiency of $\pm$1st orders with launched angle ϕ when θ equals to 0°. (d) The grating diffraction efficiency of unidirectional and bidirectional pumping mechanisms versus the pump laser wavelength.

$-$1st order rapidly drops to zero as shown in Fig. 2(c). When the launch angle ϕ is larger than $+1°$, the $+$1st order diffraction efficiency drops as the incident angle increases while the $-$1st order diffraction efficiency remains zero. Accordingly, a bidirectional pumping mechanism for a fiber laser can be achieved by aligning the pump light for normal incidence, i.e., $\theta = 0°$ and $\phi = 0°$, while the unidirectional pumping mechanism can be achieved by switching the launch angle of the pump light to $\theta = 0°$ and $\phi = 1°$. In the experiment, the switching of the launch angle required for either bidirectional pumping or unidirectional pumping can be easily accomplished by horizontally shifting the slow-axis collimation (SAC) lens array. The diffraction efficiencies for two pumping mechanisms as functions of the pump wavelength were also simulated as shown in Fig. 2(d). Considering the wavelength shift of the LDA within $\pm$5 nm around 976 nm, the influence of the central wavelength on the diffraction efficiency was not changed a lot for both bidirectional and unidirectional pump. However, the stability of the bidirectional pumping scheme is better than the unidirectional scheme since it has a smoother curve around 976 nm.

3. Fabrication

In the fabrication of the gold-embedded silica grating couplers, e-beam lithography was used to define the grating pattern, in order to achieve precise control of the dimensions of the grating grooves. Since the length of the grating coupler was designed to match the commercial 1-cm-wide laser beam of the LDA, the cascaded e-beam exposure was necessary. A 150-μm-thick fused-silica substrate was used as the substrate. A 300-nm-thick layer of e-beam resist ZEP520A was spin-coated, followed by a baking at 180 °C for 2 min. Then, a layer of 20-nm-thick charge dissipating agent, i.e., ESPACER, was spin-coated onto the resist to reduce the charging effect on the insulating substrate surface. After the grating pattern was defined, reactive ion etching (RIE) was used to etch the grating grooves into the silica substrate. During the dry etching process, O_2 plasma

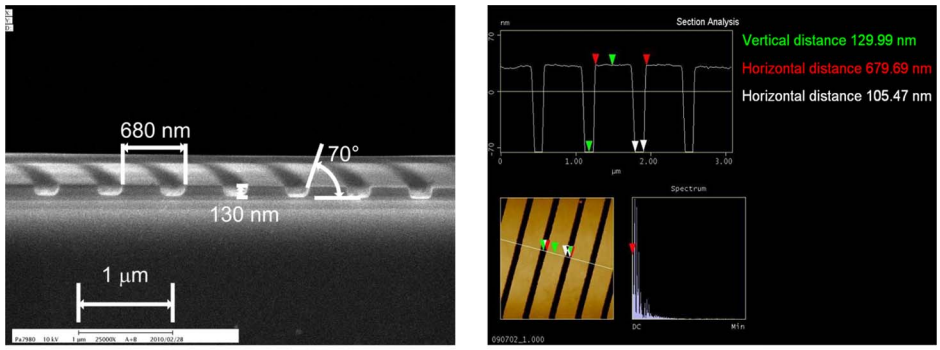

Fig. 3. (a) SEM image of the silica grating before gold deposition. Cross-sectional view reveals the trapezoid shape of the grating structure. (b) AFM contour picture of the grating with 679.69-nm pitch and 129.99-nm groove depth.

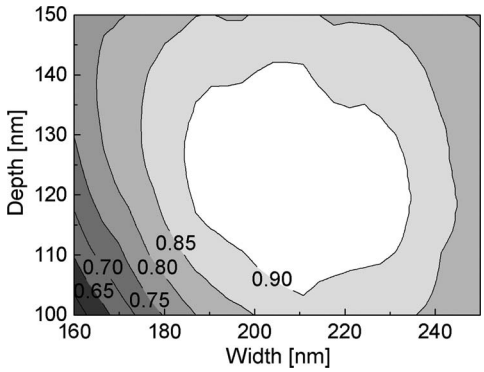

Fig. 4. Simulation of the sum of both ±1st orders diffraction efficiency as a function of the groove depth and groove width after considering the 70° sidewall angle.

was first used to remove the residual resist from the developed areas, and CHF_3 plasma was then used to remove the silica. After the etching process, the pattern for the silica grating was a negative of the pattern required gold for the embedded layer, somewhat like a mold. Finally, a 300-nm-thick layer of gold film was deposited on the silica grating mold, to form the coupler, using a thermal evaporator. The surface of the deposited gold layer for the gold-embedded silica grating coupler was then place in contact with the metal heat sink. The thermal conducting paste was applied at the contact interface to provide a low-thermal-resistance path for removing the heat generated by the optical absorption in the gold thin film. Fig. 3(a) shows the scanning electron microscope (SEM) image of the cross-sectional view of the silica grating pattern after the RIE process. An atomic force microscope (AFM) was also used to examine the groove profile as shown in Fig. 3(b). The results show that the groove depth and width were close to the design parameters, with a fabrication error of less than 3%. However, the groove walls of the fabricated grating coupler were not perfectly vertical as designed but were trapezoidal in shape with an approximately 70° angle of the sidewall, as shown in Fig. 3(a). The trapezoidal shape of the groove wall was then considered as a parameter in the numerical simulations, to determine its effect on the coupling efficiency. The contour map of the diffraction efficiency as a function of groove width and groove depth for the grating coupler with 70° groove sidewalls is shown in Fig. 4. Compared with Fig. 2(a), the optimized groove width for the grating with maximal diffraction efficiency has a slightly larger value (around 210 nm), and the optimal diffraction efficiency remains greater than 90%. This indicates that a wider groove design can be used to compensate for the effect of nonverticality in the groove wall on the diffraction efficiency.

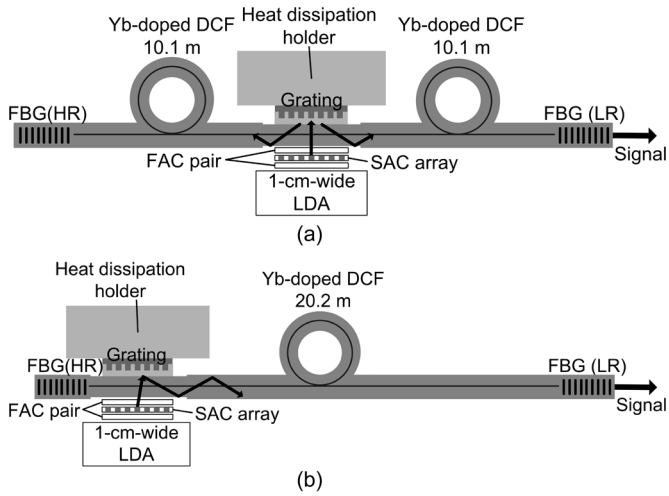

Fig. 5. Schematic diagram of side-pumped Yb-doped fiber laser. (a) Bidirectionally pumped Yb-doped fiber and (b) unidirectionally pumped Yb-doped fiber. FAC represents the fast-axis collimation lens, and SAC represents the slow-axis collimation lens.

4. Side-Pumped Fiber Lasers

The setup of the grating side-pumped fiber lasers are shown in Fig. 5. The light emission from the LDA was side pumped into the Yb-doped gain fiber through the grating coupler, and a pair of fiber Bragg gratings (FBGs) with high (99%) and low (6%) reflectivity was fused and spliced at each end of the gain fiber as the wavelength-selective reflector and output coupler, respectively. As mentioned above, the laser-pumping scheme can be switched between bidirectional pumping and unidirectional pumping by realign the pumping position to one end of the gain fiber and slightly adjusting the relative position of the SAC lens array. Fig. 5(a) and (b) represents the schematic diagrams of the bidirectionally and the unidirectionally grating side-pumped Yb-doped fiber lasers, respectively. In the experiment, the lengths of the Yb-doped gain fibers for both the bidirectional pumping and the unidirectional pumping setups are the same to facilitate the comparison of their laser performances. Because of the high-power operation, it is necessary to attach the grating coupler to a heat dissipation holder. Therefore, the massive heat generation can be rapidly transferred to the holder to avoid heat accumulation at the grating coupler.

5. Results and Discussion

To measure the light power coupled into the fiber, a pair of power meters were placed at both ends of the fiber to measure the total coupled power. Fig. 6(a) shows the measured overall coupling efficiency as the function of the groove widths at 42.4 W LDA pump power. For a grating coupler with a silica groove width of 170 nm, the coupling efficiency was only 24% with the coupled power of 10.1 W. As predicted by numerical simulation as shown in Fig. 4, the diffraction efficiency for the grating coupler with an angle of 70° side can be optimized by increasing the groove width, and the maximum efficiency occurs when the groove width is 210 nm. The black solid circular points in Fig. 6(b) represent the overall coupling efficiency against increased LDA pump power for the grating coupler with a 210-nm groove width. In this case, a total coupled power of 21 W, coupled from an LDA operated at 42.4 W, was measured, which corresponds to a coupling efficiency of approximately 50%. At a lower pump power, the coupling efficiency can even reach 66%. The temperature influence of the grating coupler was also observed while measuring the coupling efficiency as shown in Fig. 6(b). The red hollow circular and triangular points represent the temperature of the grating coupler attached on the heat dissipation holder with and without fan cooling, respectively. For the grating coupler attached on the holder without fan cooling, the temperature increases rapidly from 21 °C to 53 °C, while the pump power increases from the laser

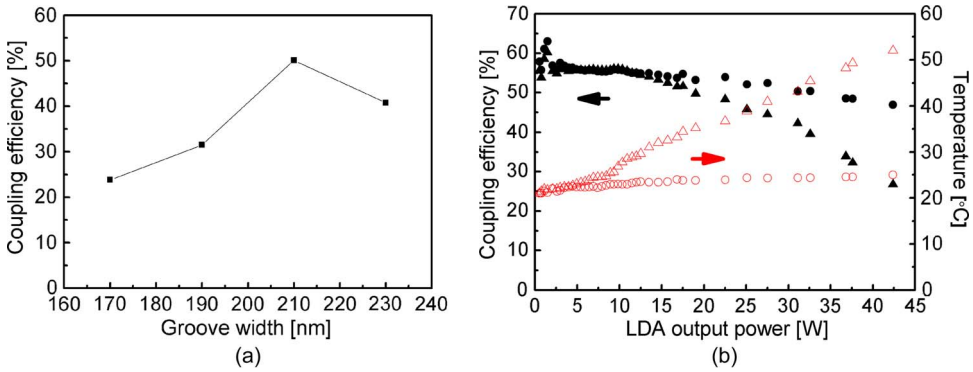

Fig. 6. (a) Overall coupling efficiency against different groove widths of the gold-embedded silica grating coupler. (b) Coupling efficiency of the grating coupler (black solid points) versus LDA output power and the temperature of heat dissipation holder (red hollow points). Circular and triangle points represent the heat dissipation holder with and without fin-type heat sink, respectively.

threshold to over 40 W. At this moment, the overall coupling efficiency drops by almost 50% as the black solid triangular points as shown in Fig. 6(b). Hence, the rapid heat removal from heat dissipation holder to the surrounding environment is still important. Besides, the efficiency peaks at the laser power of approximately 2 W, as shown in Fig. 6(b). This may be caused by a change in the spatial mode profile of the LDA. Because the LDA is a multiemitter and multimode light source, it has fewer transverse modes when the current is just above the lasing threshold. As the current increases, it abruptly evolves multiple transverse modes, because of spatial hole burning. Such an abrupt change of mode can, in turn, change the slow-axis divergence angle of the output beam, and thus change the coupling efficiency, because the diffraction efficiency of the grating is sensitive to the incident angle. Since the typical thermal expansion coefficient of silica, is approximately $5.5 \times 10^{-7}/^{\circ}\mathrm{C}$, which is quite low compared with that of gold, the relatively thermally insensitive silica mold may constrain the thermal expansion of the gold nanostructure and thus maintain the grating pitch and shape during the thermal expansion, and therefore, any decrease in coupling efficiency should be negligible.

However, the experimental result shows an appreciable slope of approximately -0.22%/W (black solid circular points) for the case with fan cooling and -0.75%/W (black solid triangular points) for the case without fan cooling, as shown in Fig. 6(b). It is caused by the back reflection of light at the grating surface feeding back to the LDA through the lenses, and then interfering with the LDA, which influences LDA output power (for either the cases with or without fan cooling), as well as the slightly deviated position of the grating coupler at high temperature caused by thermal expansion (for the case without fan cooling). The measured laser output power decreases when back reflection of light occurs. The back reflected light comes from two sources: 1) the zero-order back reflected light itself and 2) the $\pm$1st order diffraction and back reflection onto the grating coupler by the TIR at the fiber cladding boundary, which is referred to in this paper as the "backward diffraction loss." As shown in Fig. 7(a), part of the $\pm$1st order diffracted light (diffracted by the grating once) in the fiber cladding is reflected back to the grating again, resulting in a $-$1st order twice diffracted light (diffracted by the grating twice). The direction of this $-$1st order twice diffracted light is coupled out of the fiber, so the overall coupling efficiency is consequently reduced. To verify the effect of the loss caused by backward diffraction on the overall coupling efficiency, a numerical simulation was performed, in which the effect of the backward diffraction caused by the internal reflection and slow-axis divergence of the laser beam were taken into consideration. Fig. 7(b) shows the overall coupling efficiency as a function of the slow-axis divergence angle, taking losses caused by backward diffraction into account. The result shows that the overall coupling efficiency drops to approximately 70%. As the slow-axis divergence angle increases, the overall coupling efficiency drops gradually. The transition point on the curve of the overall coupling efficiency at around 6°, shown in Fig. 7(b), corresponds to propagation of the diffracted light at the critical angle of the inner

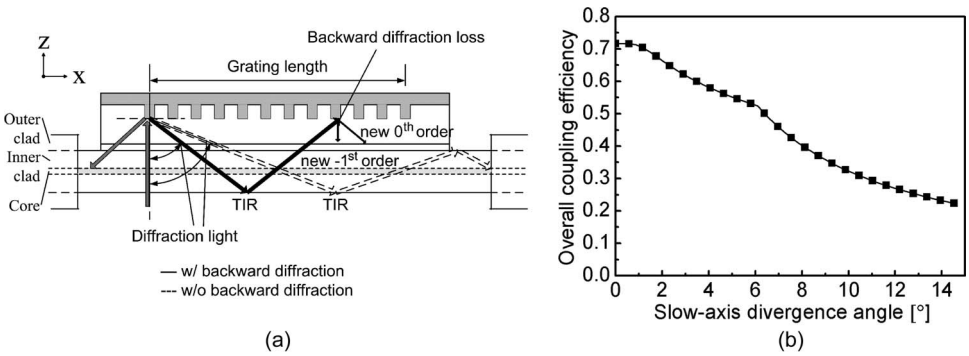

Fig. 7. (a) Schematic diagram of the backward diffraction loss. (b) Simulation of overall coupling efficiency after considering the backward diffraction loss.

TABLE 2

Pump power symmetry

SAC shift (μm)	Power of +1st order (W)	Power of -1st order (W)	Total coupled power (W)
0	9.97	9.24	19.21
30	11.95	7.31	19.26
60	13.56	5.63	19.19
90	14.51	3.52	18.03
120	14.73	0.78	15.51
150	15.00	0	15.00

cladding-air boundary. The simulation results indicate that, there are two possible ways to mitigate the loss caused by backward diffraction. First, a customized SAC lens array must be used, in order to collimate the laser beam and to ensure a divergence angle of less than 0.5°. Secondly, the grating pitch of the grating coupler must be slightly less than 680 nm to increase the diffraction angle and prevent the leaking by the grating coupler of the light already coupled in the fiber cladding.

Finally, the side-pumped fiber lasers of bidirectional and unidirectional pumping schemes were both implemented by using the grating coupler with 210-nm groove width. In one of the experiments, the LDA pump light was aligned for normal incidence to form the bidirectional side-pumped fiber laser. The power distributions of $\pm$1st order diffraction were symmetrical at normal incidence (SAC shift equals to zero). In the other experiment, the pumping scheme was switched from bidirectional pumping to unidirectional pumping by slightly adjusting the position of the SCA lens array. As the SAC lens array was being shifted, the power of $+$1st order increased, and the power of $-$1st order decreased. Table 2 shows the pump power symmetry between $+$1st order and $-$1st order at different SAC positions. The total coupled power is almost the same when the SAC shift is below 60 μm; and it starts to decrease when more SAC shift is applied. The position adjustment stopped when the power of $-$1st order dropped to zero and only the power of $+$1st order was left. At this point, the unidirectional pumping was achieved. The result shows the total coupled power for unidirectional pumping is slightly lower than that for bidirectional pumping which agrees with the theoretical analysis.

The squares and triangles shown in Fig. 8(a) represent the measured signal output power against the coupled pump power of the side-pumped Yb-doped fiber laser of bidirectional and unidirectional pumping schemes, respectively. Compared with the blue dash line and red solid line for the simulation results, it shows good agreement between the measurement results and the theoretical values. The measured laser slope efficiencies for the bidirectional pumping and unidirectional

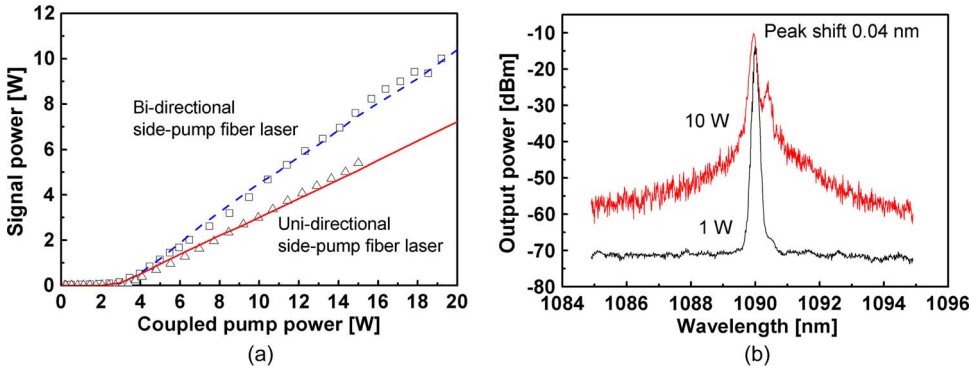

Fig. 8. (a) The measured laser signal output power against coupled pump power of bidirectional pumping (square points) and unidirectional pumping (triangular points) schemes, respectively. (b) Laser output spectrum for bidirectional pumping at 1 W (black curve) and 10 W (red curve) output power, respectively.

pumping schemes were 63% and 45%, respectively. The signal output powers were 7.7 W for bidirectional pumping and 5.4 W for unidirectional pumping when the same 15 W pump power was launched. The signal output power can even reach 10.01 W for the bidirectional side-pumped Yb-doped fiber laser while the pump power is 19.9 W. It was observed that the slope efficiency of bidirectional pumping is 18% higher than that of unidirectional pumping. The reason for the higher slope efficiency is because of the nearly optimal cavity length of bidirectional pumping. If the length of the gain fiber is too short, not all the pump power is absorbed by the gain fiber, the pump utilization is reduced. On the other hand, when the length of the gain fiber is too long, the remaining section of the gain fiber beyond a certain length may exhibit negative gain caused by weak pumping. For the unidirectional pumping scheme, the length of the gain fiber is longer than required for maintaining positive gain along the entire length, and thus, the laser slope efficiency decreases. Finally, the measured laser central wavelengths were both 1090 nm, and the laser linewidths were well below 0.02 nm because of the use of the double-clad FBGs. Fig. 8(b) shows the laser linewidth of bidirectional side-pumped Yb-doped fiber laser at different signal output power. The laser linewidth is well limited by the FBGs, and the central wavelength shifts 0.04 nm when the output power increases from 1 W to 10 W. The slight wavelength shift is reasonable for a typical fiber laser with FBGs as the wavelength selective reflectors. The obvious side-band fluctuations in the spectrum represents the larger amplified spontaneous emission at 10-W output power, and the second peak near the central wavelength is coming from the imperfect FBG spectral response.

6. Conclusion

The gold-embedded silica grating side-pumping scheme in which the light from a high-power LDA was coupled into a DCF was implemented. The experimental results show that thermal expansion caused by high-power light absorption by the metal part of the grating coupler may limit the coupling efficiency for high-power operation. In addition, the geometric parameters of the grating coupler, such as the verticality of the groove wall, the grating pitch, and the slow-axis divergence angle of the laser beam all have a significant effect on the overall coupling efficiency. The optimization of the geometric parameters for the gold-embedded silica grating coupler, taking into account the nonverticality of the groove wall and the loss caused by backward diffraction, resulted in a 25% improvement in efficiency for high-power laser operation. Up to 21 W of side-coupled pump power was coupled from the LDA into the DCF, giving an overall coupling efficiency of around 50%. Theoretically, the gold-embedded silica grating coupler can sustain a power level much higher than hundreds of watts as long as the pump power does not exceed the optical damage threshold for silica and gold. In our experimental setup, a fan-cooled heat sink was used for dissipating the heat absorbed by the metal part of the grating coupler. For a much higher pump power, the fan-cooled

heat sink could be replaced by a water-cooled heat sink with temperature control to maintain a more stable temperature of the grating coupler. Furthermore, an LDA side-pumped Yb-doped DCF laser was demonstrated by using such a grating coupler. In this kind of side-pumping scheme, the pumping direction and the pump power can be easily switched for either bidirectional pumping or unidirectional pumping without using any WDM coupler, which simplifies the complexity and reduces the cost of the entire laser construction. Finally, the signal output power of 10 W with a slope efficiency of 61% was achieved for the bidirectional side-pumped fiber laser. This preliminary experimental result shows that a much higher coupling efficiency can be achieved through the reduction of the loss caused by backward diffraction and improvement of the heat removal process for the grating coupler.

The technique demonstrated in this paper would be not only an efficient way to achieve a high-power and high-quality light source but also an possible means to construct a compact distributed side-pumped fiber laser [17], [18] that can scale up the total coupled pump power. However, in the multipoint side-pumping scheme, the pump light which is coupled from one grating coupler may leak out by the adjacent grating couplers as it is propagating through a passive fiber, but if doped active fibers (e.g., Yb-doped double clad fiber) are used instead of passive fibers and the active fiber section between any two adjacent grating couplers is long enough to allow the coupled pump light to be absorbed completely before being coupled out by the adjacent gratin coupler, the power scaling can be achieved without any pump power leakage. It should also be noted that the signal propagating in the fiber core will not leak because it is isolated from the grating coupler by the inner cladding. Besides, the technique has the advantage of mass production if the grating coupler is fabricated by using the nanoimprint techniques. Furthermore, by suitable selection of the focusing lens pair, the coupling method can be used not only for a DCF but for optical fibers with different diameters and shapes as well. Finally, the side-coupling scheme with gold-embedded silica grating coupler also has the potential for constructing a high-brightness fiber light source with a much higher power and a much more compact size by using one single high-power LD stack with cascaded LDAs, which will be our next attempt in the future.

References

[1] D. J. Richardson, J. Nilsson, and W. A. Clarkson, "High power fiber lasers: Current status and future perspectives," *J. Opt. Soc. Am. B*, vol. 27, no. 11, pp. B63–B92, Jan. 2010.

[2] E. Snitzer, H. Po, F. Hakimi, R. Tumminelli, and B. C. McCollum, "Double clad, offset core Nd fiber laser," presented at the Conf. Optical Fiber Sensors, New Orleans, LA, 1988, Paper PD5.

[3] V. Dominic, S. MacCormack, R. Waarts, S. Sanders, S. Bicknese, R. Dohle, E. Wolak, P. S. Yeh, and E. Zucker, "110 W Fibre laser," *Electron. Lett.*, vol. 35, no. 14, pp. 1158–1160, Jul. 1999.

[4] J. Limpert, A. Liem, H. Zellmer, and A. Tunnemann, "500 W continuous-wave fibre laser with excellent beam quality," *Electron. Lett.*, vol. 39, no. 8, pp. 645–647, Apr. 2003.

[5] Y. Jeong, J. K. Sahu, D. N. Payne, and J. Nilsson, "Ytterbium-doped large-core fiber laser with 1.36 kW continuous-wave output power," *Opt. Exp.*, vol. 12, no. 25, pp. 6088–6092, Dec. 2004.

[6] F. Röser, C. Jauregui, J. Limpert, and A. Tünnermann, "94 W 980 nm high brightness Yb-doped fiber laser," *Opt. Express*, vol. 16, no. 22, pp. 17 310–17 318, Oct. 2008.

[7] M. P. Kalita, S. Alam, C. Codemard, S. Yoo, A. J. Boyland, M. Ibsen, and J. K. Sahu, "Multi-watts narrow-linewidth all fiber Yb-doped laser operating at 1179 nm," *Opt. Exp.*, vol. 18, no. 6, pp. 5920–5925, Mar. 2010.

[8] P. Schreiber, B. Hoefer, P. Dannberg, and U. D. Zeitner, "High-brightness fiber-coupling schemes for diode laser bars," in *Proc. SPIE*, 2005, vol. 5876, pp. 1–10.

[9] H. G. Treusch, K. Du, M. Baumann, V. Sturm, B. Ehiers, and P. Loosen, "Fiber-coupling technique for high-power diode laser arrays," in *Proc. SPIE*, 1998, vol. 3267, pp. 98–106.

[10] H. Schlüter, C. Tillkorn, U. Bonna, G. Charache, J. Hostetler, T. Li, C. Miester, R. Roff, T. Vethake, and C. Schnitzler, "Dense spatial multiplexing enables high brightness multi-kW diode laser systems," in *Proc. SPIE*, 2006, vol. 6104, p. 61 040M.

[11] M. Haag, B. Köhler, J. Biesenbach, and T. Brand, "Novel high-brightness fiber coupled diode laser device," in *Proc. SPIE*, 2007, vol. 6456, p. 64 560T.

[12] J. J. Larsen and G. Vienne, "Side pumping of double-clad photonic crystal fibers," *Opt. Lett.*, vol. 29, no. 5, pp. 436–438, Mar. 2004.

[13] J. Xu, J. Lu, G. Kumar, J. Lu, and K. Ueda, "A non-fused fiber coupler for side-pumping of double-clad fiber lasers," *Opt. Commun.*, vol. 220, no. 4–6, pp. 389–395, May 2003.

[14] Q. Xiao, P. Yan, S. Yin, J. Hao, and M. Gong, "100 W ytterbium-doped monolithic fiber laser with fused angle-polished side-pumping configuration," *Laser Phys. Lett.*, vol. 8, no. 2, pp. 125–129, Feb. 2011.

[15] Q. Xiao, P. Yan, J. He, Y. Wang, X. Zhang, and M. Gong, "Tapered fused fiber bundle coupler capable of 1 kW laser combining and 300 W laser splitting," *Laser Phys. Lett.*, vol. 21, no. 8, pp. 1415–1419, Jul. 2011.
[16] M. G. Moharam, E. B. Grann, D. A. Pommet, and T. K. Gaylord, "Formulation for stable and efficient implementation of the rigorous coupled-wave analysis of binary gratings," *J. Opt. Soc. Amer. A.*, vol. 12, no. 5, pp. 1068–1076, May 1995.
[17] P. Yan, M. Gong, C. Li, P. Ou, and A. Xu, "Distributed pumping multifiber series fiber laser," *Opt. Exp.*, vol. 13, no. 7, pp. 2699–2706, Apr. 2005.
[18] F. Zhang, C. C. Wang, T. A. Ning, C. Liu, R. Geng, and Y. C. Lu, "Multi-point side pumping scheme of fiber lasers for high-power diode arrays," *Opt. Commun.*, vol. 282, no. 16, pp. 3325–3329, Aug. 2009.